Materials Chemistry and Physics 148 (2014) 1071–1077

Contents lists available at ScienceDirect

Materials Chemistry and Physics

journal homepage: www.elsevier.com/locate/matchemphys

ZnO and copper indium chalcogenide heterojunctions prepared by inexpensive methods

M. Berruet [a, *], Y. Di Iorio [a], M. Troviano [b], M. Vázquez [a]

[a] División Electroquímica y Corrosión, Facultad de Ingeniería, INTEMA, CONICET, Universidad Nacional de Mar del Plata, Juan B. Justo 4302, B7608FDQ Mar del Plata, Argentina
[b] Instituto de Investigación y Desarrollo en Ingeniería de Procesos, Biotecnología y Energías Alternativas (PROBIEN, CONICET-UNCo), Buenos Aires 1400, Q8300IBX Neuquén, Argentina

HIGHLIGHTS

- Heterojunctions that serve as solar cell prototypes were prepared using solution-based techniques.
- The devices comprised a double layer of ZnO and $CuInSe_2$ or $CuInSe_{0.4}S_{1.6}$.
- A TiO_2 buffer layer in the ZnO/chalcogenide interface is necessary to detect photocurrent.
- The incorporation of S improved the response of the photovoltaic heterojunction.

ARTICLE INFO

Article history:
Received 4 April 2014
Received in revised form
11 August 2014
Accepted 22 September 2014
Available online 30 September 2014

Keywords:
Chalcogenides
Optical materials
Thin films
Solar cells

ABSTRACT

Solution-based techniques were used to prepare ZnO/CuIn(Se, S)$_2$ heterojunctions that serve as solar cell prototypes. A duplex layer of ZnO (compact + porous) was electrodeposited. Chalcogenide thin films were deposited using successive ionic layer adsorption and reaction method (SILAR). By subsequent thermal treatments in two different atmospheres, $CuInSe_2$ (CISe) and $CuInSe_{2-x}S_x$ (CISeS) were obtained. The composition and morphology of the annealed films were characterized by GXRD, micro-Raman spectroscopy and SEM.

Devices prepared with CISe and CISeS show a clear photo-response. The introduction of a buffer layer of TiO_2 into the ZnO/chalcogenide interface was necessary to detect photocurrent. The presence of CISeS improves the response of the cell, with higher values of short circuit current density, open circuit potential and fill factor. These promising results show that it is possible to prepare photovoltaic heterojunctions by depositing chalcogenides onto porous ZnO substrates using low-cost solution-based techniques.

1. Introduction

Thin film solar cells based on chalcopyrite compounds attract permanent interest. For terrestrial applications, cost-effective deposition techniques and large area processing are key factors. Thus, electrodeposition and chemical bath techniques have been chosen to prepare laboratory prototypes of thin film solar cells. ZnO has been widely applied to different architectures of solar cells both as an n-type semiconductor or window layer. $CuInSe_2$ (CISe) and $CuInS_2$ (CIS) are good candidates for photovoltaic applications given their high absorption coefficients (greater than 10^4 cm^{-1}) and appropriate band gap energy values (1.1 eV for CISe and 1.4 eV for CIS). In a superstrate configuration, ZnO can act as the n-type component of the junction while $CuInSe_2$ or $CuInSe_{2-x}S_x$ (CISeS) act as the p-type, absorbing layer. But when ZnO has to be used a substrate for the solution-based deposition of a second material, the amphoteric nature of ZnO, and the ease with which ZnO dissolves in acidic and basic solutions, may become a problem. Previous works have shown that the incorporation of an anatase film may act a barrier and prevent the chemical degradation of ZnO during the subsequent deposition of the chalcogenide film [1,2]. In a previous work we prepared a solar cell depositing $CuInS_2$ by spray pyrolysis onto an electrodeposited ZnO double layer with a

* Corresponding author. División Electroquímica y Corrosión, INTEMA, UNMdP, CONICET, Juan B. Justo 4302, B7608FDQ Mar del Plata, Argentina.
E-mail addresses: berruetm@gmail.com, mberruet@fi.mdp.edu.ar (M. Berruet).

http://dx.doi.org/10.1016/j.matchemphys.2014.09.019
0254-0584/

blocking layer of TiO_2 between them. Another way of tackling this drawback is by adjusting the conditions for the chalcogenide deposition technique, so that it can be carried out within the pH window where ZnO remains stable.

Solar cells incorporating both types of chalcopyrites prepared using diverse non-vacuum techniques have already been reported [3]. Among them electrodeposition [4–6], spraying [7–9] and solution growth techniques [10,11] can be mentioned as examples. In many cases, a thermal treatment in highly toxic H_2S is required [12]. Instead, our approach involves reactive sulfurization of the CuSe and In_2Se_3 precursors, prepared by a chemical bath method in near neutral–pH aqueous solution [2].

In this work, CISe is deposited onto a double layer of ZnO by successive ionic layer adsorption and reaction method (SILAR), where a sequence of heterogeneous reactions between the solid phase and the solvated ions in the solution leads to a solid state mixture of CuSe and In_2Se_3. If these selenides are heated up to 400 °C in argon atmosphere, CISe is formed. But if sulfur vapor is introduced in the chamber, some Se atoms are replaced by S atoms and a quaternary compound (CISeS) is formed. The main advantages of this method are the optimum material utilization, the possibility of controlling the film thickness, the chance of choosing different substrates and a large-scale deposition capability.

Single films of ZnO, CISe and CISeS have been thoroughly characterized previously [2,13,14]. This work, in contrast, will focus on the analysis of the junction, as a potential candidate for a photovoltaic solar cell. In particular, the influence of the chalcogenide composition on the energy conversion efficiency of solar cells prototypes will be evaluated. The porous nature of ZnO and the cyclic character of SILAR may contribute in forming a pn junction distributed in space. Although a photo induced response has been detected, it proved necessary to incorporate a thin layer of TiO_2 to act as buffer layer so improving the performance of the cell.

2. Material and methods

2.1. Substrate

Glass coated with a transparent conducting tin oxide (FTO, SnO2:F, Libbey Owens Ford, TEC 8/3: resistivity 8 Ω/sq, thickness 600 nm) was used as substrate. Prior to use, the substrates were degreased with detergent solution and then rinsed in an ultrasonic bath with ethanol and acetone during 10 min respectively. The substrate was cut into square pieces (2 × 2 cm^2) and the active geometrical area was limited to 1.22 cm^2 by the electrochemical cell design.

2.2. ZnO electrodeposition

A double layer of compact and porous ZnO was electrodeposited using aqueous solutions and a standard, three-electrode cell configuration. A saturated calomel electrode (SCE) was used as reference and a Pt mesh of big area as counter electrode. All the experiments are carried out using a Voltalab PGP 201 potentiostat. To deposit the compact layer (co-ZnO), the electrolytic bath consisted of aqueous solutions of 0.1 mol/L $Zn(NO_3)_2$ and 0.1 mol/L KNO_3 (pH = 5). ZnO was deposited at 60 °C, holding the electrode at −1.2 V vs. SCE up to a final charge density of 0.13 C/cm^2, equivalent to a thickness of 100 nm according to Faraday's law. The films were annealed at 450 °C for 40 min in air. A porous layer of ZnO (po-ZnO) was electrodeposited on top of the compact layer. This was prepared from an aqueous solution containing 0.1 mol/L $Zn(NO_3)_2$, 0.1 mol/L KNO_3 and 4 g/L polyvinylpyrrolidone K 30 (PVP K 30) used as surfactant. The electrodeposition was carried out at 60 °C, fixing the potential at −1.1 V vs. SCE up to a final charge density of 1.2 C/cm^2, equivalent to a thickness of 900 nm according to Faraday's law. The electrodeposited oxide obtained was then annealed at 380 °C for 40 min in air.

2.3. TiO_2 buffer layer

Buffer layers are known to assist carrier transport or improve band alignment. A thin layer of CdS is frequently incorporated in CIGS, CISe and CdTe-based solar cells. However, due to the contaminant nature of Cd compounds, alternative films have also been used. In this case, a TiO_2 film was deposited by spray pyrolysis. A precursor solution containing titanium IV isopropoxide (TTIP) was used as titanium source, acetylacetone (AcAc) as a stabilizer and ethanol as solvent. More details of the experimental procedure can be found elsewhere [15].

2.4. CISe/CISeS deposition

CISe thin films were deposited on FTO/ZnO and FTO/ZnO/TiO_2 using a chemical method known as successive ionic layer adsorption and reaction (SILAR). The cationic precursor solution was prepared from two separated solutions, one containing 0.06 mol L^{-1} indium chloride ($InCl_3$) complexed with 0.06 mol L^{-1} sodium citrate (CitNa) and the other 0.06 mol L^{-1} cupric chloride ($CuCl_2$) complexed with 0.6 mol L^{-1} triethanolamine (TEA). These are then mixed, stirring continuously during 1 h. The anionic precursor solution was prepared by refluxing and stirring 0.025 mol Se and 0.05 mol Na_2SO_3 in 0.25 L deionized water at 100 °C during 2 h. The solutions are prepared using AR grade chemicals.

Each dipping cycle proceeded at 80 °C and included 30 s immersions in the cationic and anionic precursor solutions and 20 s rinsing stages. Each cycle was repeated 70 times.

During each cycle CuSe and In_2Se_3 are deposited. If the films are annealed during 90 min at 450 °C in argon atmosphere, CISe is formed, as described by reaction (1).

$$2\,CuSe + In_2Se_3 \rightarrow 2\,CuInSe_2 + Se \quad (1)$$

If sulfur powder is added during the annealing stage, CISeS forms as described by reaction (2).

$$2\,CuSe + In_2Se_3 + 2x\,S \rightarrow 2\,CuInSe_{2-x}S_x + (1+2x)Se \quad (2)$$

More details on the preparation of the solution have been given previously [13].

After annealing, secondary phases were removed by immersion in a 0.5 mol L^{-1} KCN solution during 20 s. Finally, the samples were subjected to soft annealing by holding them at 200 °C during 120 min in air.

2.5. Characterization

The films were analyzed by X-ray diffraction using a PANalytical X'Pert Pro diffractometer, Cu-Kalpha radiation at 40 kV and 40 mA. The samples were scanned using grazing incidence, between 20° and 80° at 0.02°/s. The crystallographic data for each phase were taken from the literature and analyzed with X'Pert HighScore software.

Raman spectra were performed using an Invia Reflex confocal Raman microprobe. Excitation is provided with the 514 nm emission line of an Ar + laser. The measurements were carried out in backscattering configuration using a 50× objective.

The morphology of the layers was studied with scanning electron microscopy (SEM), using a JEOL JSM-6460LV microscope. Cross-section images of the films were obtained using a Focused-Ion Beam Scanning Electron Microscope (Auriga Cobra FIB SEM).

The thicknesses of the films were measured using a KLA TENCOR D-100 profilometer.

Photoelectrochemical (PEC) characterizations were carried out in a standard three-electrode cell together with a Pt mesh as counter electrode and a saturated calomel electrode (SCE) as reference. The experiments were performed at room temperature and the solutions were bubbled with nitrogen during 30 min previous to use. The working electrode area was 1.41 cm^2. The light source was a 150 W Xe lamp coupled to an air-mass filter 1.5G (solar simulator, Oriel-Newport 96000). Photocurrent and photopotential were evaluated forming a semiconductor/electrolyte junction by immersion of the FTO/ZnO and FTO/CISe films in a 0.2 mol L^{-1} KCl solution. The light was chopped using an electronic shutter (Uniblitz model T132) with an ON/OFF period of 10 s.

To evaluate the photoelectric response of solar cell prototypes, such as that presented in Fig. 1, current–voltage curves were performed in the dark and under illumination. The graphite contacts were painted onto the samples with conductive graphite ink. Electrode area (3 mm^2) was defined using a mask. The graphite electrode was the working electrode, while the FTO film served as the counter/reference electrode. Thus, in forward bias, the graphite film was positive relative to the FTO electrode. An IVIUM® compact potentiostat was employed to carry out these measurements.

3. Results and discussion

3.1. Duplex ZnO/chalcogenide: composition, morphology and thickness

ZnO is an example of an amphoteric oxide that can dissolve in acidic and alkaline solutions. In these cells prototypes, a duplex layer of ZnO (compact + porous) is electrodeposited on FTO. Later, this layer serves as substrate for the chemical deposition of CISe or CISeS. This deposition involves successive immersions in the anionic and cationic precursor solutions described in Section 2.1. Thus, keeping in mind the amphoteric nature of ZnO, it is important to verify that this layer remains stable and does not dissolve while depositing the chalcogenide by the SILAR method.

For this purpose, GXRD diffractograms are shown in Fig. 2 which correspond to samples containing $CuInSe_2$ and $CuInSe_{2-x}S_x$, deposited onto FTO/ZnO substrates. Two important issues can be observed in this figure. First, the characteristic peaks of the chalcopyrite structure (highlighted in gray) are present in both diffractograms, such as (112), (204/220), and (116/312). The peaks are narrow and their relative intensity is similar to those in the diffraction cards of $CuInSe_2$ (PDF 40–1487) and $CuInS_2$ (PDF 27–0159). As presented in a previous work [2], sulfurization shifts the chalcopyrite reflections of pure CISe toward the positions characteristic of pure CIS, which is taken as proof for the formation of the quaternary compound, $CuInSe_{2-x}S_x$. The position of the characteristic peaks of the quaternary phase depends on the percentage of S atoms replacing Se atoms, which ends up being 80%. The magnification shown in Fig. 2 is centered in the signal from plane (112) corresponding to highest intensity peak. Unfortunately, plane (112) in $CuInSe_2$ is overlapped with plane (110) from FTO (PDF 77–0450). In spite of being superimposed, the shift in the signal that results from sulfurization can be clearly seen.

Additionally, the presence of a layer of ZnO below the layer of the chalcogenide can be confirmed. ZnO patters present a hexagonal structure matching that the wurtzite (PDF 79–0209). All of the peaks are present and preserve a good relation of intensities, demonstrating that ZnO remains stable after the chalcogenide has been deposited. Finally, the diffractograms show some unlabeled

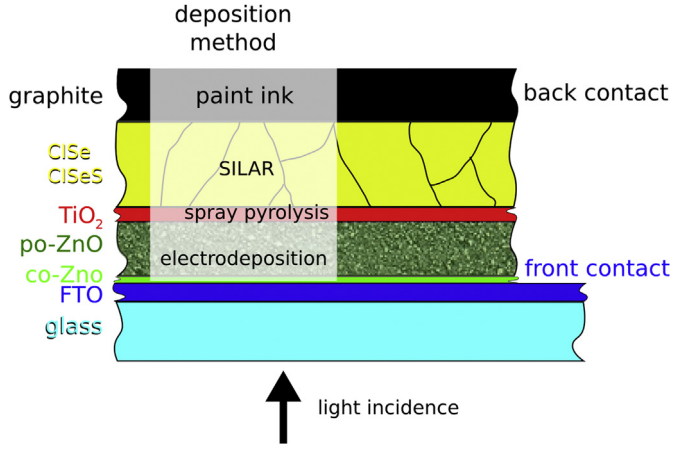

Fig. 1. Graphical scheme of the ZnO/chalcogenide solar cell prototype in superstrate configuration.

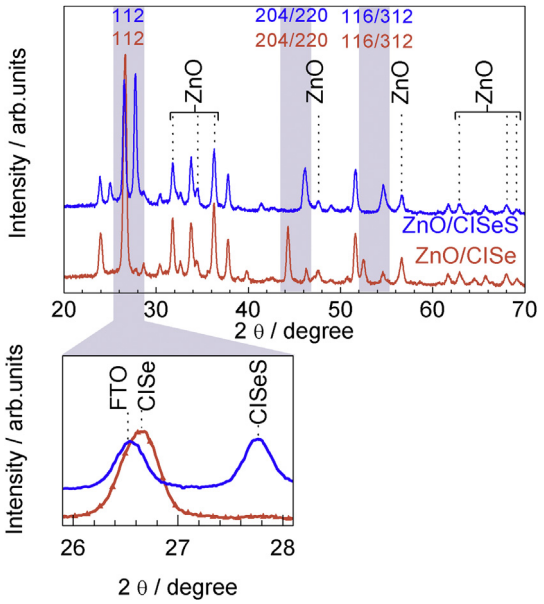

Fig. 2. Grazing incidence X-ray diffractogram of CISeS (upper line) and CISe (lower line) deposited on glass/FTO/co-ZnO/po-ZnO substrates. The insert shows a magnification of the (112) diffraction plane. Unlabeled peaks correspond to FTO diffraction planes and k_β radiation from the X rays that cannot be filtered.

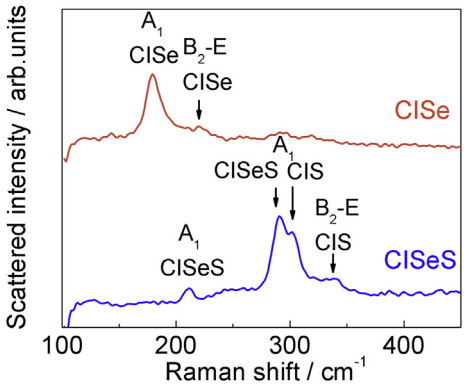

Fig. 3. Raman spectra of CISe (upper line) and CISeS (lower line) films deposited onto FTO/ZnO substrates.

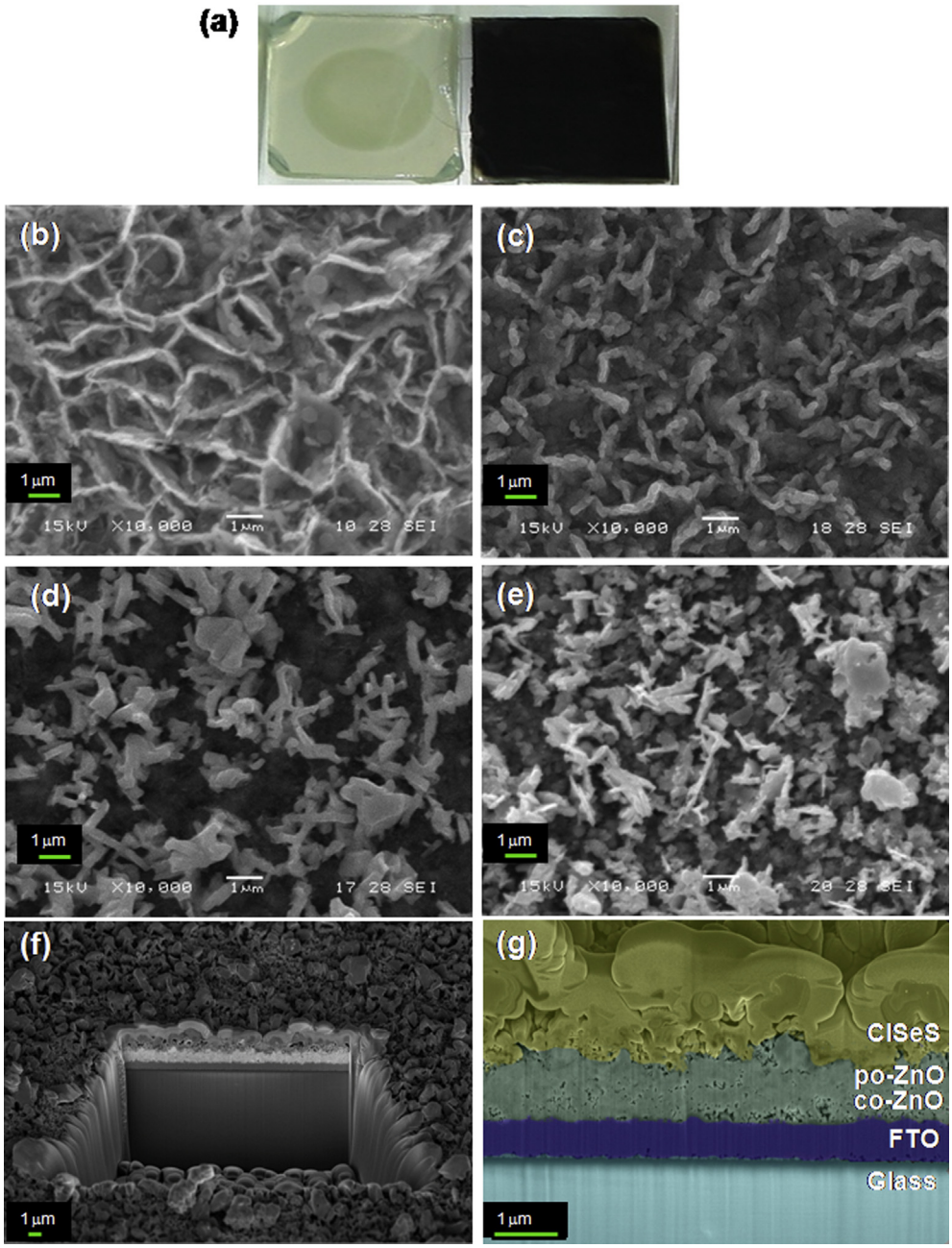

Fig. 4. (a) Photographs of the double layer of ZnO deposited onto FTO substrate (left) and $CuInSe_2$ on top of them (right). (b) SEM micrograph of po-ZnO deposited on top of FTO/co-ZnO, (c) SEM micrograph of TiO_2 blocking layer deposited on top of po-ZnO and the chalcogenides (d) SEM micrograph of CISe and (e) CISeS deposited on top of TCO/ZnO/TiO_2. (f) FIB-SEM micrograph of milling FTO/co-ZnO/po-ZnO/CISeS layers. (g) Cross section FIB-SEM of FTO/co-ZnO/po-ZnO/CISeS layers.

peaks that correspond to k_β radiation from the X rays that cannot be filtered because of the incidence angle.

Fig. 3 shows Raman spectra of the chalcogenides (CIS and CISeS) deposited onto FTO/ZnO. Samples annealed in Ar (CISe) present the A_1 mode peak at 173 cm^{-1} related to the vibration of Se–Se bonds (anions) and weak peaks at 220 cm^{-1}, typical of the Cu–In bonds in CISe [16]. After sulfurizing (i.e. in CISeS), the signals that correspond to the A_1 mode from CIS (300 cm^{-1}) and CISe (173 cm^{-1}) now shift to 290 cm^{-1} and 210 cm^{-1}, respectively. This bimodal behavior is typical of a CISeS quaternary phase and has been labeled as A_1 CISeS in Fig. 3. Similar results have also been reported in the literature [17]. The other bands in the Raman spectrum can be attributed to characteristic modes of the CIS, such as the A_1 mode at 300 cm^{-1} and the B_2–E mixed mode at 330 cm^{-1}. These results are in good agreement with previously published report in which chalcogenide thin films were deposited on FTO and glass substrates [13].

Fig. 4 shows images of the ZnO and the CISe/CISeS layers. Fig. 4a presents two photographs of the double layer of ZnO deposited onto FTO substrate (left) and $CuInSe_2$ on top of them (right). Then, SEM micrographs of porous ZnO deposited on top of FTO/co-ZnO can be seen in Fig. 4b, TiO_2 blocking layer deposited on top of porous ZnO in Fig. 4c and the chalcogenides CISe and CISeS deposited on top of TCO/ZnO/TiO_2 in Fig. 4d, e, respectively. Finally, the last two photos correspond to cross sectional FIB-SEM images for FTO/ZnO/CISeS layers, as can be seen in Fig. 4f, g. All the films present good coverage and a homogeneous structure. The presence

of the surfactant in the electrodeposition bath is clearly responsible for the open porous structure of ZnO, which is presented in Fig. 4b. Then, small particles of TiO_2 deposited onto ZnO seem to copy the morphology of that porous structure, as can be seen in Fig. 4c. The morphology of CISe and CISeS resembles sub-micron platelets, similar to those reported in previous work [13], which were deposited on bare glass (not shown). Here, the difference is that the morphology of CISe tends to be more open than that of CISeS.

FIB-SEM cross-sectional views of FTO/co-ZnO/po-ZnO/CISeS are shown in Fig. 4f, g. It can be seen that although CISeS presents an open structure, the interface of both materials is completely connected. Thereby, SILAR deposition seems to be an appropriated technique to cover the entire surface and even fill the structured ZnO to enhance interconnection. The images illustrate average effective thicknesses of the ZnO film (830 nm) and the CISeS (1400 nm) absorbing layer. Due to the high roughness of CISeS films it is not possible to measure the effective thickness using a profilometer. Table 1 shows the thickness of each layer of ZnO measured using different methods: a profilometer, cross sectional FIB-SEM images and Faraday's law. Faraday's law thickness results for compact ZnO are in agreement with those measured using the profilometer but underestimate that of porous ZnO. This can be explained taking into account the bulk density has been used while applying Faraday's law. Also, it can be seen that profilometer values added for compact and porous ZnO, remain higher than the FIB-SEM value. There are several arguments that can explain the discrepancy. In Fig. 4g there are multiple layers present, not just plain ZnO. It is possible that the chalcogenide may be penetrating hundreds of nanometers into ZnO and the microscope resolution is unable to solve the boundary. Another possibility is that ZnO is partially dissolved after being in contact with precursor solutions of the SILAR method. Previously, it had been demonstrated by XRD and FIB-SEM that electrodeposited ZnO layer is conserved after the deposition of CISe or CISeS. Nevertheless, these techniques cannot rule out partial dissolution.

3.2. Electrical properties

Photoelectrochemistry can be used to elucidate the nature of the carriers. The main effect of periodic illumination on the current driven by semiconductor electrodes under potentiostatic control is the creation of electron–hole pairs, which modifies the concentration of minority carriers and thereby promotes processes governed by the minority carrier concentration. During photoexcitation, both photopotential and photocurrent can be observed. The photoexcited electrons and holes are separated in the space charge region (SCR), with each moving in opposite directions across the electric field. This movement induces an inverse potential in the electrode (photopotential) which reduces the potential difference across the space charge region and retards the migration of the carriers. In the case of n-type semiconductors, the Fermi level of the semiconductor increases (the electrode potential decreases) when the band edge level bends upward in the space charge region. Moreover, photocurrent is registered when the holes photoproduced in the space charge region move towards the electrode/electrolyte interface and increase the anodic current. In the case of p-type semiconductors, an equivalent but opposite reasoning applies. The carrier movement is schematically illustrated in Fig. 5.

The photopotential and the photocurrent registered at open circuit potential (OCP) for FTO/co-ZnO/po-ZnO (5a) and FTO/CISe (5b) layers in a 0.2 mol L^{-1} KCl solution is also presented in Fig. 5. With illumination, the potential moves to negative or positive values for the ZnO and CISe – electrolyte interface, respectively. In parallel, with illumination the current moves in the positive or negative direction for ZnO and CISe – electrolyte interface, respectively. These shifts confirm the n-type and p-type nature of the ZnO and CISe films. The same behavior was observed for CISeS (not shown).

Comparing the response of both systems, it can be observed that Fig. 5a shows a rapid response when light is on, where a new steady state is achieved before 10 s of illumination. However, the photopotential cycles obtained for CISe (Fig. 5b) need longer times to

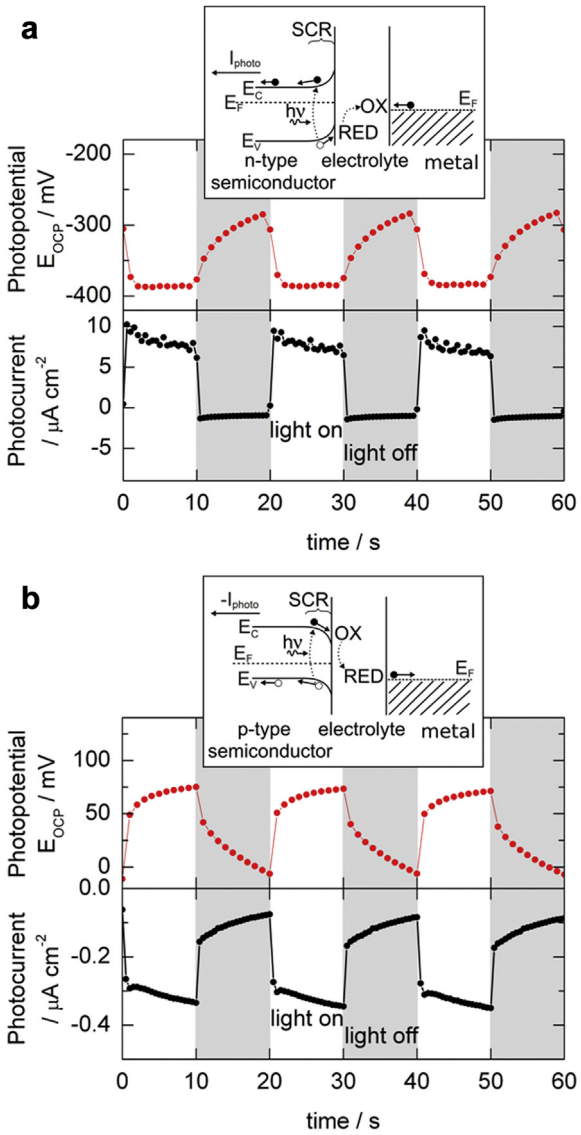

Fig. 5. Evolution of photopotential (top) and photocurrent (bottom) in time of (a) FTO/co-ZnO/po-ZnO/electrolyte/Pt and (b) FTO/CISe/electrolyte/Pt. Potential values were recorded versus SCE reference electrode at open circuit potential. 0.2 mol L^{-1} KCl was used as electrolyte. The inserts show schematic diagrams for the band structure of the semiconductor/electrolyte interface.

Table 1
Thickness values of co-ZnO and po-ZnO layers measured using different methods: Faraday's law, cross sectional FIB-SEM images and a profilometer.

Method	co-ZnO/nm	po-ZnO/nm
From Faraday's law	100	900
Profilometer	130	1600
FIB-SEM	830	

stabilize. This behavior could be explained by a lower mobility of charge carriers in $CuInSe_2$.

To complete the characterization of the ZnO/chalcogenide junction, two prototypes of solar cells were constructed. Since a simple FTO/ZnO/$CuInSe_{2-x}S_x$ structure showed photo induced response without a photocurrent signal being detected (not shown), a buffer layer of TiO_2 was introduced. Finally, graphite paste was applied to make back-contacts (in the area of 3 mm^2) on top of the CISeS absorber.

Current density–voltage (J–V) responses, in the dark and under illumination, are shown in Fig. 6 for two types of devices, FTO/ZnO/TiO_2/CISe/graphite (Fig. 6a) and FTO/ZnO/TiO_2/CISeS/graphite (Fig. 6b). The only difference between them is the chalcogenide composition (thermal treatment performed with or without sulfur present in the chamber).

All samples and spots in each FTO/ZnO/TiO_2/CISeS/graphite heterojunction have an identical response confirming reproducibility and homogeneity. In contrast, a few spots in the FTO/ZnO/TiO_2/CISe/graphite heterojunction show ohmic behavior, possibly due to the more open structure of CISe. In this case, best device response is shown.

The dark response for the two devices shows diode behavior with good rectification ratios although the current density differs in an order of magnitude, being higher for ZnO/TiO_2/CISeS. Under illumination the presence of CISeS improves the response of the heterojunction. This is reflected in the higher values of short circuit current density (J_{sc}), open circuit potential (V_{oc}) and fill factor (FF) as shown in Fig. 7. No efficiency values have been reported because they were lower than 1%.

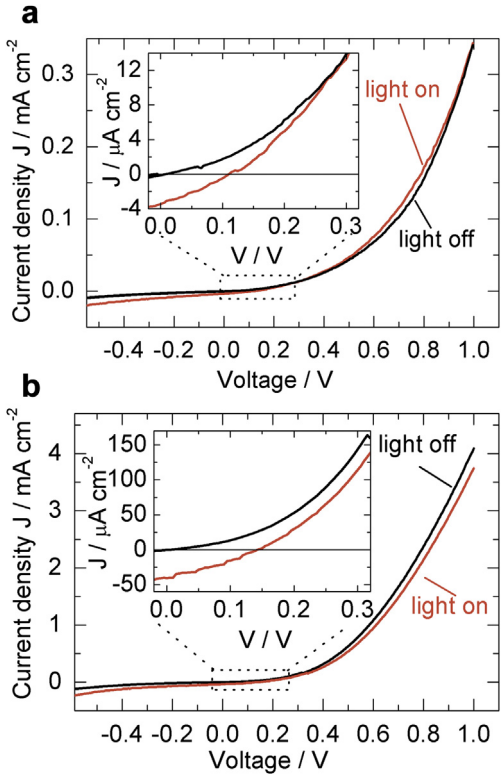

Fig. 6. J–V response of two cell configurations in the dark (black line – light off) and under simulated solar irradiation (red line – light on). (a) FTO/ZnO/TiO_2/CISe/graphite and (b) FTO/ZnO/TiO_2/CISeS/graphite. The insert shows a magnification of the active photocurrent area. (For interpretation of the references to color in this figure legend, the reader is referred to the web version of this article.)

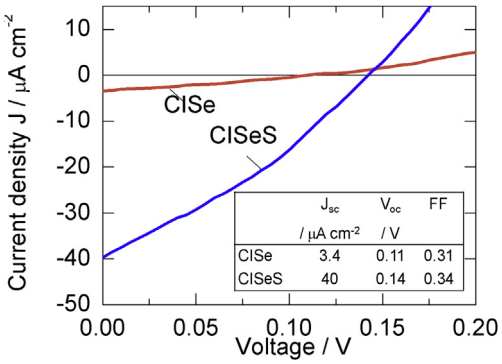

Fig. 7. J–V response of FTO/ZnO/TiO_2/CISe/graphite (orange line – CISe) and FTO/ZnO/TiO_2/CISeS/graphite (blue line – CISeS) cell configuration under simulated solar irradiation. The inserted table shows values for J_{sc}, V_{oc} and FF in the two configurations. (For interpretation of the references to color in this figure legend, the reader is referred to the web version of this article.)

Normally, in CIS/CISe devices prepared by inexpensive methods, the shape of the J–V curve obtained under illumination does not reflect a simple downwards shift of the dark I–V curve in vertical direction [2,5,9], which can be expected according to the shifting approximation. Also, at higher bias voltage, the dark and light J–V characteristics intersect, known as the crossover phenomenon and frequently found in CIS devices [18]. Interestingly, this situation is present in the CISe device shown in Fig. 6a but not in the CISeS device (Fig. 6b). This could suggest a difference in device quality. In CIGS devices prepared by conventional sputtering of the layers, distortion in the current density–voltage curves can be caused by non-ohmic back-contacts, and deep level defects in the absorber, the buffer layer, and at the absorber/buffer interface [19].

On the other hand, both heterojunctions showed low values for the short circuit current density, open circuit potential and fill factor, which can be attributed to different reasons. A similar situation was reported before for co-TiO_2/po-TiO_2/CISeS heterojunctions obtained by spray pyrolysis, doctor blade and SILAR respectively [2]. Small currents could be attributed to fast hole–electron recombination in the p-n junction which, in turn, could be due to different types of defects induced by deposition techniques. Also, the thicknesses of absorber and window layers may not be optimal. Finally, the presence of series and shunt resistances within the multilayer structure or a misalignment of the bands cannot be discarded.

4. Conclusions

ZnO/CISe and ZnO/CISeS heterojunctions have been prepared using solution-based techniques, in particular electrodeposition for the oxide bi-layer and the SILAR method for the chalcogenide. The SILAR method has been optimized to achieve a homogeneous chalcogenide layer while preventing ZnO dissolution.

By controlling the atmosphere of the thermal treatment, two compositions of the chalcogenide have been tested: $CuInSe_2$ and $CuInSe_{0.4}S_{1.6}$. With both of them, the heterostructures show a clear photo-response. To detect photocurrent, a buffer layer of TiO_2 has to be introduced between ZnO and CISeS, resulting in an FTO/co-ZnO/po-ZnO/TiO_2/CISeS/graphite structure. When comparing CISe with CISeS it has been found that the incorporation of S improves the response of the cell, with higher values of short circuit current density (J_{sc}), open circuit potential (V_{oc}) and fill factor (FF). The results presented above can be taken as a first step in the right direction. Many experimental variables may be adjusted to improve the efficiency in the energy conversion, in particular the resistivity

and thickness of the semiconductor layers. Also, the etching time and etchant concentration are important parameters that influence the final Cu/In ratio in these films.

Although further optimization to improve the photovoltaic performance is necessary, it has been demonstrated that this all-solution process has a potential for developing low-cost ZnO/CISeS solar cells.

Acknowledgments

The authors acknowledge the financial support received from the Consejo Nacional de Investigaciones Científicas y Técnicas (CONICET) and Universidad Nacional de Mar del Plata, both from Argentina. We are also grateful to Eng. Orofino for the profilometer measurements and Dr. Malwela for the FIB-SEM measurements.

References

[1] M. Law, L.E. Greene, A. Radenovic, T. Kuykendall, J. Liphardt, P. Yang, J. Phys. Chem. B 110 (2006) 22652–22663.
[2] M. Berruet, M. Valdés, S. Ceré, M. Vázquez, J. Mater. Sci. 47 (2012) 2454–2460.
[3] N. Naghavi, D. Abou-Ras, N. Allsop, N. Barreau, S. Bücheler, A. Ennaoui, C.H. Fischer, C. Guillen, D. Hariskos, J. Herrero, R. Klenk, K. Kushiya, D. Lincot, R. Menner, T. Nakada, C. Platzer-Björkman, S. Spiering, A.N. Tiwari, T. Törndahl, Prog. Photovolt. Res. Appl. 18 (2010) 411–433.
[4] J. Kois, M. Ganchev, M. Kaelin, S. Bereznev, E. Tzvetkova, O. Volobujeva, N. Stratieva, A.N. Tiwari, Thin Solid Films 516 (2008) 5948–5952.
[5] M. Valdés, M.A. Frontini, M. Vázquez, A. Goossens, Appl. Surf. Sci. 254 (2007) 303–307.
[6] M. Valdés, A. Goossens, M. Vázquez, Mat. Chem. Phys. 125 (2011) 860–865.
[7] H. Yoon, J.H. Woo, B. Joshi, Y.M. Ra, S.S. Yoon, H.Y. Kim, S.J. Ahn, J.H. Yun, J. Gwak, K.H. Yoon, S.C. James, J. Electrochem. Soc. 159 (2012) H444.
[8] T. Theresajohn, M. Mathew, C. Sudhakartha, K. Vijayakumar, T. Abe, Y. Kashiwaba, Sol. Energy Mater. Sol. Cells 89 (2005) 27–36.
[9] M.H. Valdés, M. Berruet, A. Goossens, M. Vázquez, Surf. Coat. Technol. 204 (2010) 3995–4000.
[10] S. Ahn, T.H. Son, A. Cho, J. Gwak, J.H. Yun, K. Shin, S.K. Ahn, S.H. Park, K. Yoon, ChemSusChem 5 (2012) 1773–1777.
[11] C.R. Kim, S.Y. Han, C.H. Chang, T.J. Lee, S.O. Ryu, Curr. Appl. Phys. 10 (2010) S383–S386.
[12] Y. Lai, S. Kuang, F. Liu, Z. Yuan, Z. Zhang, Y. Li, J. Liu, B. Wang, D. Tang, J. Li, Y. Liu, Appl. Surf. Sci. 257 (2011) 8360–8365.
[13] M. Berruet, W.H. Schreiner, S. Ceré, M. Vázquez, J. Alloys Compd. 509 (2011) 3019–3024.
[14] M. Berruet, M. Vázquez, Mater. Sci. Semicond. Process. 13 (2010) 239–244.
[15] M. Valdés, M. Vázquez, A. Goossens, Electrochim. Acta 54 (2008) 524–529.
[16] V. Izquierdo-Roca, X. Fontané, L. Calvo-Barrio, A. Pérez-Rodríguez, J.R. Morante, J. Álvarez-García, F. Duault, L. Parissi, V. Bermúdez, Thin Solid Films 517 (2009) 2264–2267.
[17] S. Shirakata, T. Terasako, T. Kariya, J. Phys. Chem. Solids 66 (2005) 1970–1973.
[18] E. Kärber, A. Abass, S. Khelifi, M. Burgelman, A. Katerski, M. Krunks, Sol. Energy 91 (2013) 48–58.
[19] C.-H. Chung, B. Bob, T.-B. Song, Y. Yang, Sol. Energy Mater. Sol. Cells 120 (2014) 642–646.